Interfering with aggregated α-synuclein in advanced melanoma leads to a major upregulation of MHC class II proteins

Claudia Fokken[a,*], Ivan Silbern[b,c,*], Orr Shomroni[d,*], Kuan-Ting Pan[b], Sergey Ryazanov[a], Andrei Leonov[a], Nadine Winkler[a], Henning Urlaub[b,c], Christian Griesinger[a,e] and Dorothea Becker[a,f]

Melanoma is the most serious and deadly form of skin cancer and with progression to advanced melanoma, the intrinsically disordered protein α-synuclein is upregulated to high levels. While toxic to dopaminergic neurons in Parkinson's disease, α-synuclein is highly beneficial for primary and metastatic melanoma cells. To gain detailed insights into this exact opposite role of α-synuclein in advanced melanoma, we performed proteomic studies of high-level α-synuclein-expressing human melanoma cell lines that were treated with the diphenyl-pyrazole small-molecule compound anle138b, which binds to and interferes with the oligomeric structure of α-synuclein. We also performed proteomic and transcriptomic studies of human melanoma xenografts that were treated systemically with the anle138b compound. The results reveal that interfering with oligomerized α-synuclein in the melanoma cells in these tumor xenografts led to a substantial upregulation and expression of major histocompatibility complex proteins, which are pertinent to enhancing anti-melanoma immune responses. *Melanoma*

***Res* 34: 393–407 Copyright © 2024 The Author(s). Published by Wolters Kluwer Health, Inc.**

Melanoma Research 2024, **34**:393–407

Keywords: α-synuclein, advanced melanoma, MHC class II antigen upregulation

[a]Department of NMR-based Structural Biology, Max Planck Institute for Multidisciplinary Sciences, [b]Bioanalytical Mass Spectrometry Group, Max Planck Institute for Multidisciplinary Sciences, [c]Bioanalytics Research Group, Institute of Clinical Chemistry, University Medical Center Göttingen, [d]NGS-Integrative Genomics Core Unit (NIG), Institute of Human Genetics, University Medical Center Göttingen, [e]Cluster of Excellence 'Multiscale Bioimaging: from Molecular Machines to Networks of Excitable Cells' (MBExC), Georg-August-University Göttingen and [f]Institute for Organic and Biomolecular Chemistry, Georg-August-University Göttingen, Göttingen, Germany

Correspondence to Dorothea Becker, PhD, Department of NMR-based Structural Biology, Max Planck Institute for Multidisciplinary Sciences, Am Fassberg 11, 37077 Göttingen, Germany
Tel: +49 551 201 2200; e-mail: dbecker@mpinat.mpg.de

*Claudia Fokken, Ivan Silbern, and Orr Shomroni contributed equally to the writing of this article.

Received 16 March 2024 **Accepted** 3 May 2024.

Introduction

Over the past several years, the treatment landscape of advanced melanoma has changed and improved significantly due to immune checkpoint inhibitors administered alone or in combination. However, the 5-year survival rate of patients with advanced melanoma, having received immune checkpoint inhibitor combination therapy with an anti-PD-1 or anti-CTLA-4 antibody, is still only about 50% [1,2].

By now, it is well documented that autophagy plays an important role in the advanced stages of melanoma, that is, in primary and metastatic melanoma, but not in noninvasive melanoma in situ [3,4]. To date, interfering with or inhibiting autophagy in advanced melanoma has been explored primarily in the context of in vitro studies and in mouse models of melanoma [5,6]. Furthermore, only a limited number of clinical trials [https://clinicaltrials.gov/ (search terms: All studies; Melanoma; Autophagy)] have been conducted thus far, to determine whether targeting autophagy in advanced melanoma with for example, the lysosomal inhibitor hydroxychloroquine alone or in combination with a small-molecule inhibitor targeting BRAF, MEK, or AKT has efficacious anti-melanoma activity.

Aberrant pathological aggregation of α-synuclein is the hallmark of the neurodegenerative diseases Parkinson's disease, multiple system atrophy, and dementia with Lewy bodies. A substantial number of studies have shown that patients with Parkinson's disease have a low risk of developing a malignancy with the exception of melanoma ([7] and references therein). Previously, we provided experimental evidence that α-synuclein promotes and thereby, is highly beneficial to the survival of melanoma in its advanced stages because it functions as a pertinent rheostat for melanoma cell autophagy, which is a major survival mechanism for primary and metastatic melanoma cells [8].

Related digital media are available in the full-text version of the article at www.melanomaresearch.com.

Supplemental Digital Content is available for this article. Direct URL citations appear in the printed text and are provided in the HTML and PDF versions of this article on the journal's website, www.melanomaresearch.com.

To obtain detailed insights into the molecular changes occurring in advanced melanoma when this rheostat role of α-synuclein is being interfered with or abolished, we performed the following studies: (i) proteomic analysis of paired high-level α-synuclein-expressing human melanoma cells that had been treated with the anle138b compound, which binds to and interferes with oligomeric but not monomeric α-synuclein [9,10]; (ii) liquid chromatography-tandem mass spectrometry (LC-MS/MS) and whole transcriptome sequencing (RNA-seq) of metastatic human melanoma xenografts had been treated systemically with the anle138b compound. Integrated analysis of the proteomics data of the anle138b-treated primary and metastatic melanoma cells showed that expression of proteins, important in the organization of the extracellular matrix and proteins implicated in mitophagy were upregulated. In the case of the systemically anle138b-treated human melanoma xenografts, highly upregulated, both at the level of the proteome and transcriptome, were MHC class II proteins.

In light of the fact that low, or loss, of expression of MHC class I/MHC class II antigens and therefore, immune escape is a distinct feature of advanced melanoma, our findings presented here, suggest that interfering with/disabling the autophagy-guarding rheostat function of α-synuclein in advanced melanoma may enhance the efficacy of immune checkpoint inhibitor-based therapies.

Methods

Human melanoma cell lines and xenografts

The human melanoma cell lines WM983-A and WM983-B were propagated in vitro and non-treated or treated with anle138b as previously described [8]. Carried out under approved Niedersächsisches Landesamt für Verbraucherschutz und Lebensmittelsicherheit (LAVES) protocol (33.19-42502-04-14/1724), WM983-B human melanoma xenografts were generated bilaterally in 4–5 weeks old female nude mice (CAnN.Cg-Foxn1nu/Crl) (Charles River Laboratories, Sulzfeld, Germany). When the tumors had reached a size of 2.3–3.0 mm in any direction, the tumor-bearing animals were randomized into two groups and for 10–16 days, one group of mice, comprised of eight animals, was given a food pellet diet containing anle138b (2 g of anle138b/kg of food pellets) and the other group, comprised of six mice, a food pellet diet not containing anle138b. Thereafter, a section from the center of each resected and cryopreserved WM983-B tumor xenograft was analyzed by analytical high performance liquid chromatography as previously described [8].

Sucrose density gradient ultracentrifugation and immunoblot analysis

Stock solutions of anle138b were made in dimethyl sulfoxide (DMSO). WM983-B melanoma cells that had received serum-free culture medium containing DMSO only or anle138b (10 μM) for 72 h, with replenishment of an equivalent dose of the diphenylpyrazol (DPP) compound at 48 h, were lysed for 30 min on ice in a buffer containing 50 mM Tris pH 7.4, 175 mM NaCl, 0.1% Nonidet P-40 substitute (Merck, Taufkirchen, Germany), EDTA-free protease inhibitor cocktail (Roche), and PhosSTOP phosphatase inhibitor (Roche). After removal of cell debris by centrifugation, total protein cell lysates (400 μg each) were fractionated by sucrose density gradient ultracentrifugation (10–60% w/v sucrose), followed by successive collection of the fractionated protein samples, their precipitation by trichloroacetic acid, and subsequent immunoblot analysis with a 1 : 1000 dilution of a rabbit anti-human mAb [MJFR1] to α-synuclein (Abcam, Cambridge, UK). Intensity of the protein signals on the immunoblots was quantified with the ImageJ image processing software (National Institutes of Health, Bethesda, Maryland, USA).

ELISA assay

Serum-free cell culture supernatants, collected from WM983-B melanoma cells that had received DMSO only, or were treated for 48 h or 72 h with rapamycin (0.5 μM) or anle138b (10 μM), with replenishment of the equivalent dose of rapamycin or anle138b at 48 h, were centrifuged twice, and 100 μl of each cell culture supernatant, diluted 1 : 4 with PBS containing 0.1% Tween-20 and 1% BSA, was added to 96-well plates that had been coated with an antibody to human α-synuclein antibody [MJFR1] (Abcam). Following a 2 h incubation at room temperature (RT), and subsequent addition of a mouse anti-α-synuclein antibody [clone 42/α-synuclein] (BD Biosciences, Heidelberg, Germany), an anti-mouse HRP-conjugated antibody (GE Healthcare, Braunschweig, Germany), and 3,3′,5,5′-tetramethylbenzidine chromogenic substrate, reactions were stopped with 1 M sulfuric acid (H_2SO_4). Sample absorbance was measured at 450 nm in an Infinite 200 PRO microplate plate reader (Tecan, Männedorf, Switzerland).

Mass spectrometry-based proteomics analysis

For the MS-based proteomics analysis of the serum-free cell culture supernatants from the WM983-B melanoma cells that for 48 h or 72 h had been treated with anle138b or with rapamycin, or had received DMSO or serum-free cell culture medium only, the collected supernatant media as well as the serum-free cell culture medium were centrifuged twice. Following methanol-chloroform precipitation of 100 μl from each collected supernatant, each protein pellet was reconstituted in 100 mM triethylammonium bicarbonate (TEAB) buffer, pH 8.0 that contained 1% RapiGest SF (Waters GmbH, Eschborn, Germany).

WM983-A as well as WM983-B melanoma cells, that had been treated with anle138b or had received DMSO only, were rinsed twice with PBS, lysed in 50 mM TEAB buffer, pH 8.0, containing 150 mM NaCl, 0.5% NP40, and 1× cOmplete EDTA-free protease inhibitor cocktail and sonicated in a BioRuptor (Diagenode, Seraing, Belgium).

Following reduction and alkylation with 10 mM tris(2-carboxyethyl)phosphine at 55 °C for 30 min and 18.75 mM iodoacetamide for 20 min at RT, the protein lysates were acetone-precipitated, and the pellets were reconstituted in 1% RapiGest SF in 100 mM TEAB buffer, pH 8.0.

Snap-frozen WM983-B melanoma xenograft tissues were homogenized in lysis buffer (100 mM HEPES, pH 8.0, 4% SDS, 1 mM EDTA, 1× cOmplete EDTA-free protease inhibitor cocktail) and with zirconia/glass beads in a bead beating grinder (FastPrep24; MP Biomedicals, Eschwege, Germany). The lysates were sonicated for 5 min in a BioRuptor with 30 s on-and-off cycles for 5 min, and cleared by centrifugation for 10 min at 17 000 *g*. Except for the proteins in the various cell culture supernatants, the dissolved proteins were digested with trypsin, labeled with tandem mass tag TMTsixplex label reagent, desalted, and in the case of the WM983-B melanoma xenograft tissue samples, pre-fractionated as previously described [11].

Liquid chromatography-tandem mass spectrometry data acquisition and analysis

For LC-MS/MS data acquisition, we used either a Q Exactive HF-X (Thermo Fisher Scientific, Waltham, Massachusetts, USA) or an Orbitrap Fusion Lumos Tribrid (Thermo Fisher Scientific) mass spectrometer, and an LC setup as described [11]. Ninety-min LC gradients were used for the proteins in the cell culture supernatants, elongated 180 min LC gradients for the WM983-A and WM983-B melanoma cell line samples, and 90 min LC gradients for the pre-fractionated tumor xenograft samples. The instruments were operated in the data-dependent acquisition mode using either a standard MS^2 or an SPS-MS^3 method [12].

Raw LC-MS/MS data were processed with MaxQuant software (version 1.5.5.1) (https://www.maxquant.org/) using default settings if not specified otherwise. MS/MS spectra were searched against *Homo sapiens* and, in the case of the WM983-B tumor xenograft tissue samples, additionally, against *Mus musculus* canonical protein sequences derived from UniProt. MS^2 or MS^3 TMT6 reporter ion intensities were selected for protein quantification where applicable. Following analyses was conducted using R software. In brief, protein groups with at least two razor or unique peptides were considered for quantification. For TMT6-labeled samples, reporter ion intensities were log2-transformed and normalized by log2-median subtraction. Differential expression analysis was performed using the *limma* R/Bioconductor software package (https://www.bioconductor.org/). *Q*-values were computed based on the *limma*-moderated *P*-values. Candidate proteins were selected satisfying the criteria: *q*-value <0.05 or moderated *P*-value <0.01 and absolute log2 intensity fold change (log2FC) > log21.5. For the proteome analysis of the WM983-A and WM983-B melanoma cell line samples, log2FC in the anle138b-treated cells versus the cells that received DMSO only or were nontreated, were subjected to hierarchical clustering using *hclust* function in R. Only protein groups satisfying minimum intensity threshold of log2 (iBAQ) > 22 were used for the analysis. For proteins identified in the cell culture supernatants of the anle138b-, rapamycin-, and DMSO-treated WM983-B melanoma cells, protein intensities were derived from the respective 'iBAQ' column in the 'proteinGroups.txt' table reported by MaxQuant. Only proteins quantified based upon at least two unique or razor peptides and not abundant (<1% of total protein intensity) in the cell culture medium control were analyzed further. Log2FC in proteins intensity were computed between each treated sample and the respective control samples. Log2FC of protein groups, quantified in the cell culture supernatants of the WM983-B melanoma cells that had been treated for 48 h or 72 h with anle138b or rapamycin and satisfied the threshold of log2FC > 1, were subjected to hierarchical clustering using *hclust* function in R. Protein interaction and functional enrichment analyses were performed using the STRING database with its evidence mode active interaction sources: Textmining, Experiments, Databases, and Co-occurrence.

RNA extraction, cDNA library construction, and RNA-seq

Total RNA from the cryopreserved control and anle138b-treated WM983-B human melanoma xenografts were extracted with TRIzol reagent. Quality of the isolated RNAs was determined on a Bioanalyzer 2100 Fragment Analyzer (Agilent, Santa Clara, California, USA) and on a NanoDrop ND-1000 spectrophotometer. A TruSeq RNA Library Prep Kit v2 (Illumina, San Diego, California, USA) was used to prepare cDNA libraries, and following quantitation of the cDNA libraries with a QuantiFluor dsDNA System (Promega, Walldorf, Germany) and determination of the size of the cDNA libraries with a dsDNA 905 Reagent Kit (Agilent), the cDNA libraries were sequenced on an Illumina HiSeq 4000 System (Illumina).

Bioinformatics analysis

Raw read and quality check: Sequence images were transformed with Illumina software BaseCaller to BCL files, which were demultiplexed to fastq files with bcl2fastq v2.17.1.14. Sequence quality was asserted using FastQC (http://www.bioinformatics.babraham.ac.uk/projects/fastqc) version 0.11.5. *Mapping and normalization*: In the case of the WM983-B melanoma tumor xenograft tissue samples, the obtained sequences were aligned to reference genome *Homo sapiens* (hg38 version 97, https://www.ensembl.org/Homo_sapiens/Info/Index) and to reference genome *Mus musculus* (mm10 version 97, https://www.ensembl.org/Mus_musculus/Info/Index). For both sets of samples, alignment was performed using the STAR

aligner [13] version 2.5.2a, which allows two mismatches within 50 bases. Thereafter, read counting was performed using featureCounts [14] version 1.5.0-p1. Read counts were analyzed in the R/Bioconductor environment (version 3.6.1, www.bioconductor.org) using the DESeq2 [15] version 1.24.1. Gene annotations were performed using *Homo sapiens* and *Mus musculus* entries via biomaRt R package version 2.40.5 [16]. Concerning the human melanoma tumor-xenograft tissue samples, proteins in the anle138b-treated versus the nontreated tumor tissue samples were considered to be significantly different in their level of expression when they had an adjusted *P*-value less than or equal to 0.05, and an absolute log2FC equal to or greater than 0.5.

Live-cell imaging

WM983-B melanoma cells seeded in 96-well black plates, received 24 h later serum-free culture medium containing DMSO only, or 10 µM of anle138b. Forty-eight hours later, the culture medium was replaced with serum-free culture medium containing 10 µM of anle138b or DMSO only and in each case, 500 nM of the 5-580CP-Hoechst dye. Following a 60-min incubation of the cells at 37 °C, live-cell imaging was performed with an LSM880 Airyscan confocal microscope (Zeiss, Carl Zeiss Microscopy Deutschland GmbH, Oberkochen, Germany) on the ZEN platform. Images of the melanoma cells, stained with the Hoechst DNA dye, were acquired with a 20× objective and in Z-stack mode every 10 min for 90 cycles (total acquisition time ~15 h). Each video (in .mp4 format) was created from a quadrant of a single Z-stack tile image.

Immunoblot analysis

For the analysis of IL-8, QPCT, stearoyl-CoA desaturase (SCD) (SCD1), farnesyl diphosphate synthase (FDPS), or fibronectin 1 (FN1) expression, WM983-B melanoma whole-cell lysates were separated on 12% SDS-PAGE and transferred onto polyvinylidene difluoride or nitrocellulose membrane. After cross-linking with 0.4% paraformaldehyde in PBS and blocking with 5% powdered milk, the membranes were probed with antibody against IL-8 (Abcam), QPCT (Novus Biologicals, Centennial, Colorado, USA), SCD1 (Abcam), FDPS (Novus Biologicals), or FN1 (Abcam), followed by incubation with an HRP-conjugated secondary antibody and Clarity Western ECL Substrate (Bio-Rad, Feldkirchen, Germany). Protein loading was determined by secondary probing with an anti-GAPDH (Abcam) or an anti-vinculin (Novus Biologicals) antibody.

Immunohistochemistry

Five-µm tissue sections, prepared from cryopreserved WM983-B human melanoma xenografts, were fixed with 4% paraformaldehyde, blocked with 10% goat serum in PBS, and probed with rabbit anti-human antibody against CRYAB (Abcam), ALDH1A1 (Abcam), FN1 (Abcam), or MHC class II (HLA-DPB1) (Abcam). Subsequently, all tissue sections were probed with a goat anti-rabbit Alexa Fluor 488-conjugated secondary antibody, counterstained with fluorescent DAPI, followed by addition of Mowiol mounting medium. Images of the tissue sections, probed with antibody to CRYAB, ALDH1A1, or MHC class II protein were acquired with a 40×/1.4 oil immersion objective on a Zeiss LSM780 laser scanning confocal microscope. Images of the tissue sections probed with an antibody to FN1 were acquired with a Plan Neofluar 20×/0.50 objective on a Zeiss Axioplan 2 fluorescence microscope. The ImageJ image processing software was used to measure cell fluorescence and to calculate corrected total cell fluorescence quantitation (CTCF) of expression of the proteins CRYAB, ALDH1A1, and MHC II in tissue sections prepared from WM983-B human melanoma xenografts.

Five-µm tissue sections, prepared from cryopreserved WM983-B human melanoma xenografts, were fixed with 4% paraformaldehyde in PBS, treated with a 1× solution of TrueBlack lipofuscin autofluorescence quencher (Biotium, Fremont, USA), blocked with 10% goat serum in PBS and probed with a mouse anti-human antibody cocktail to the three melanoma cell markers MART-1, tyrosinase, and gp100 (Novus Biologicals) or with a 1 : 150 dilution of an antibody to human α-synuclein [MJFR1] (Abcam). Thereafter, the tissue sections were probed with a goat anti-mouse or goat anti-rabbit DyLight 755 secondary antibody (Novus Biologicals), counterstained with fluorescent DAPI, followed by addition of Fluoromount-G mounting medium. Images of the tissue sections were acquired with a 40×/0.95 air objective on a SLIDEVIEW VS200 research slide scanner (Evident) and thereafter, processed with OlyVIA-Software (Evident).

Four melanoma tissue microarray (TMA) slides (https://www.biomax.us/tissue-arrays/Melanoma/ME811), each containing two tissue sections from the same 39 cases of melanoma, and tissue sections from three cases of normal skin tissue were heated at 60 °C, deparaffinized and rehydrated. After heat-induced antigen retrieval, the slides were submerged in a 0.3% Sudan Black solution to reduce autofluorescence, followed by addition of blocking solution. Thereafter, one of the TMA slides was incubated overnight with an anti-human α-synuclein antibody [MJFR1] (Abcam), a second TMA slide with a rabbit anti-human MHC class II (HLA DQ/DR/DP [HLA-Pan/2967R]) antibody (Novus Biologicals), and a third TMA slide with a mouse mAb [EMR8-5] to human MHC class I (HLA-ABC) protein (Abcam) and subsequently probed with a goat anti-rabbit or an anti-mouse DyLight 755-conjugated secondary antibody, and counterstained with DAPI solution. The slides were mounted with Fluoromount-G mounting medium. The fourth TMA slide was stained with hematoxylin and eosin and mounted with Entellan (Merck). Images of the TMA

cores were acquired with a 20×/0.80 air objective on a SLIDEVIEW VS200 research slide scanner (Evident) and thereafter, processed with OlyVIA-Software (Evident). The QuPath bioimage analysis software [17] was used to quantify the fluorescence intensity of areas marked in tissue sections of four of the TMA cores probed with α-synuclein, MHC class II, or MHC class I antibody, respectively.

Results

Anle138b treatment of metastatic melanoma cells interferes with their α-synuclein aggregates, leads to the release of α-synuclein into the extracellular milieu, and restricts the cells' dynamic properties

To determine whether anle138b interferes with aggregated α-synuclein in high-level α-synuclein-expressing melanoma cells, we performed an experiment involving sucrose-gradient centrifugation followed by immunoblot analysis of the metastatic melanoma cell line WM983-B, which as we previously showed, expresses high levels of α-synuclein compared to some other metastatic melanoma cell lines [8]. The results of this analysis (Fig. 1a) show that following treatment of these cells with anle138b, high-molecular oligomerized α-synuclein was reduced and shifted towards low-molecular weight oligomers.

Since previously, it had been shown that oligomeric forms of α-synuclein can be found in multiple extracellular fractions, associated with exosomes and free, and that the pathway of secretion of α-synuclein oligomers is strongly influenced by autophagic activity [18], we treated the WM983-B melanoma cells with anle138b and likewise, with the macrolide antibiotic rapamycin, an inhibitor of the mechanistic Target Of Rapamycin Complex 1 [19], which is a pertinent regulator of autophagy. Depicted (Fig. 1b) are the results of an ELISA, which show that a 48-h treatment with a single 10 μM dose of anle138b led to the release of α-synuclein into the cell culture supernatant, which was further increased at 72 h following addition of a second 10 μM dose of anle138b at 48 h. In comparison, treatment of these melanoma cells with the autophagy inducer, rapamycin, did not lead to a substantial release of α-synuclein into the cell culture supernatant (Fig. 1b).

Furthermore, the analysis of the MS-based proteomics data of the serum-free cell culture supernatants from the anle138b- versus the rapamycin-treated WM983-B melanoma cells revealed that both at the 48 h and the 72 h time-point, the proteins that were released upon anle138b versus rapamycin treatment were considerably different (Fig. 1c and d). For example, treatment of the melanoma cells with a single 10 μM dose of anle138b for 48 h led to release of the microtubule depolymerizing protein stathmin 1 (STMN1) and the heat shock protein HSPB1 (Hsp27), which prevents the aggregation of mutant forms of α-synuclein [20]. Following anle138b treatment of the WM983-B melanoma cells for 72 h, released into cell culture supernatant was the Tripartite motif-containing 28 (TRIM28) protein, which as a binding partner of the melanoma-associated antigen-A3/A6 (MAGE-A3/A6) has been shown to inhibit autophagy [21], and in high-level TRIM28-expressing melanomas to correlate with a significant depletion of tumor-infiltrating immune cells [22]. Another protein that was released from the melanoma cells upon treatment with the anle138b compound for 72 h was the actin- and myosin-binding protein caldesmon (CALD1).

To visualize, over a period of about 15 h, the dynamic events occurring in the WM983-B melanoma cells treated with a 10 μM dose of anle138b for 48 h, followed by replenishment with another 10 μM dose at 48 h, we stained the cells with the 5-580CP-Hoechst DNA dye [23] and thereafter, performed live-cell imaging. As can be seen in Fig. 2 (please see videos online), compared with WM983-B melanoma cells that had received DMSO only (Fig. 2a), the morphological features of the anle138b-treated melanoma cells (Fig. 2b) were noticeably different, that is, their cytoplasm showed extensive vacuolization, and some of the cells failed to divide.

Anle138b treatment leads to significant changes in the proteome of primary and metastatic human melanoma cells

To obtain information whether treatment with the DPP compound anle138b led to changes at the level of the proteome in melanoma cells expressing high levels of α-synuclein, we treated the high-level α-synuclein-expressing melanoma cell lines WM983-A and WM983-B, which were derived from a primary melanoma and a metastasis of a same patient, for 72 h with 10 μM of anle138b with replenishment of the compound (10 μM) at 48 h. Hierarchical clustering of the identified proteome changes revealed five clusters of proteins (Fig. 3a) that both in the primary and in the metastatic melanoma cells were upregulated or downregulated compared with the same melanoma cells that had received cell culture medium containing or not containing DMSO.

For validation of the proteomics data/proteins identified in these clusters, we chose two proteins from clusters 4 and 5 that were upregulated and one protein each from cluster 1 and cluster 3 that were downregulated. The results of immunoblot analyses (Fig. 3b) demonstrated that following a 72 h treatment of the WM983-B metastatic melanoma cells with anle138b, IL-8 (CXCL8) and likewise, glutaminyl-peptide cyclotransferase (QPCT) were upregulated. Expression of the pro-inflammatory cytokine IL-8 is upregulated to high levels with progression from melanoma in situ to metastatic melanoma [24,25] and although a direct interaction between IL-8 and α-synuclein has not been reported, it has been shown that serum levels of IL-8 correlate positively with clinical

Fig. 1

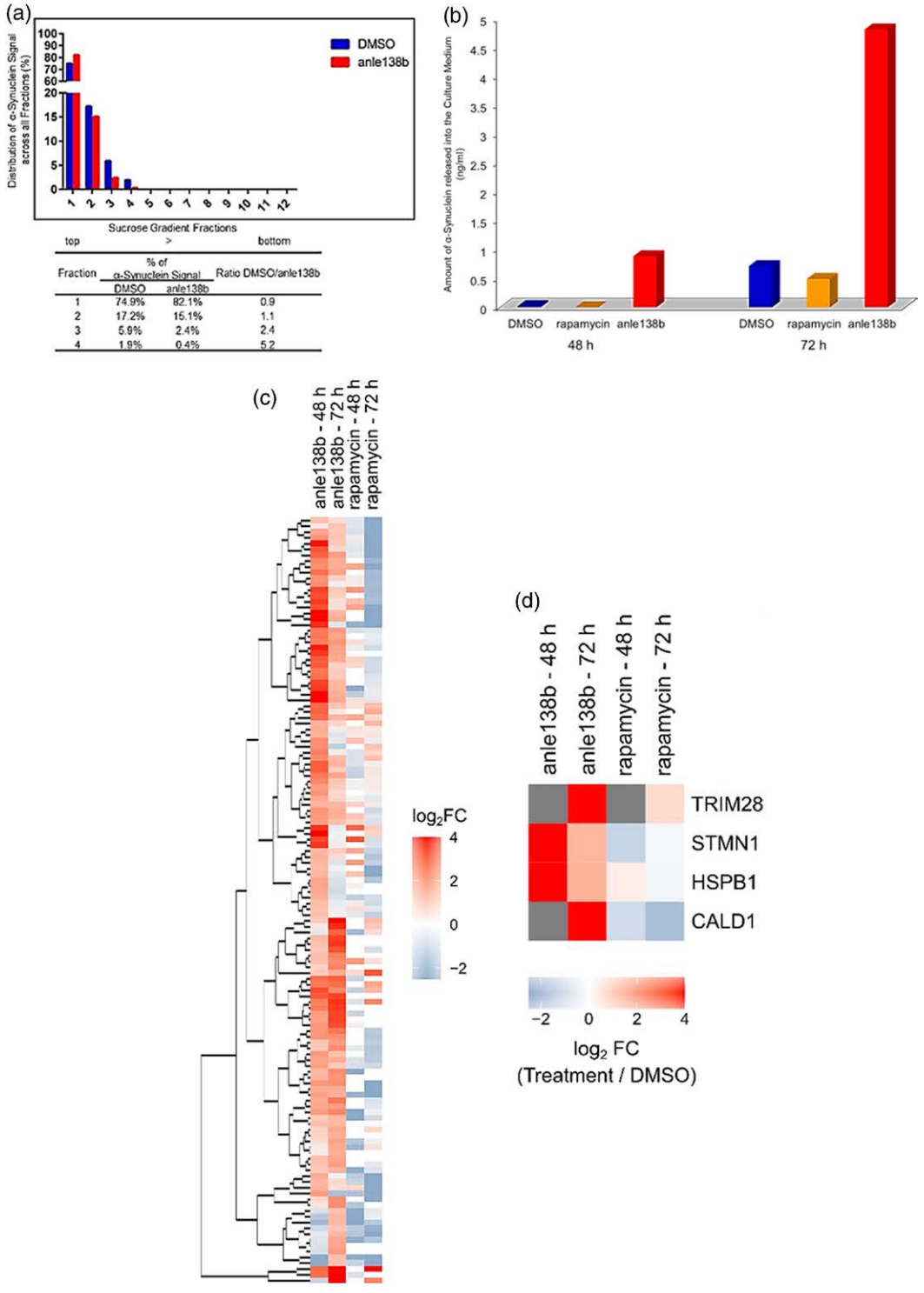

Treatment of melanoma cells with anle138b leads to a reduction in oligomerized α-synuclein and release of α-synuclein into the cell culture supernatant. (a) Sucrose density gradient fractionation followed by immunoblot analysis of α-synuclein expression in whole-cell lysate of WM983-B melanoma cells that had received DMSO only, or were treated with 10 μM of anle138b for 72 h, with replenishment of 10 μM of the compound at 48 h. Representative experiment shown, $n = 1$. (b) ELISA analysis of the presence of α-synuclein protein in serum-free cell culture supernatant of WM983-B cells that had received DMSO only, or were treated with 0.5 μM of rapamycin or 10 μM of anle138b for 48 h or 72 h, with replenishment of an equivalent dose of rapamycin or anle138b at 48 h. Shown for each time point is the mean of duplicate samples analyzed, $n = 1$. (c) Clusters of proteins, identified by MS-based proteomics analysis, that were released at the 48 h and the 72 h time-point into the serum-free cell culture supernatants of the anle138b- versus the rapamycin-treated WM983-B melanoma cells. (d) Log2FC of four select proteins identified by MS-based proteomics, in the serum-free cell culture supernatants of WM983-B melanoma cells that were treated for 48 h and 72 h with anle138b or rapamycin, with replenishment of an equivalent dose of anle138b or rapamycin at 48 h. DMSO, dimethyl sulfoxide; MS, mass spectrometry.

Fig. 2

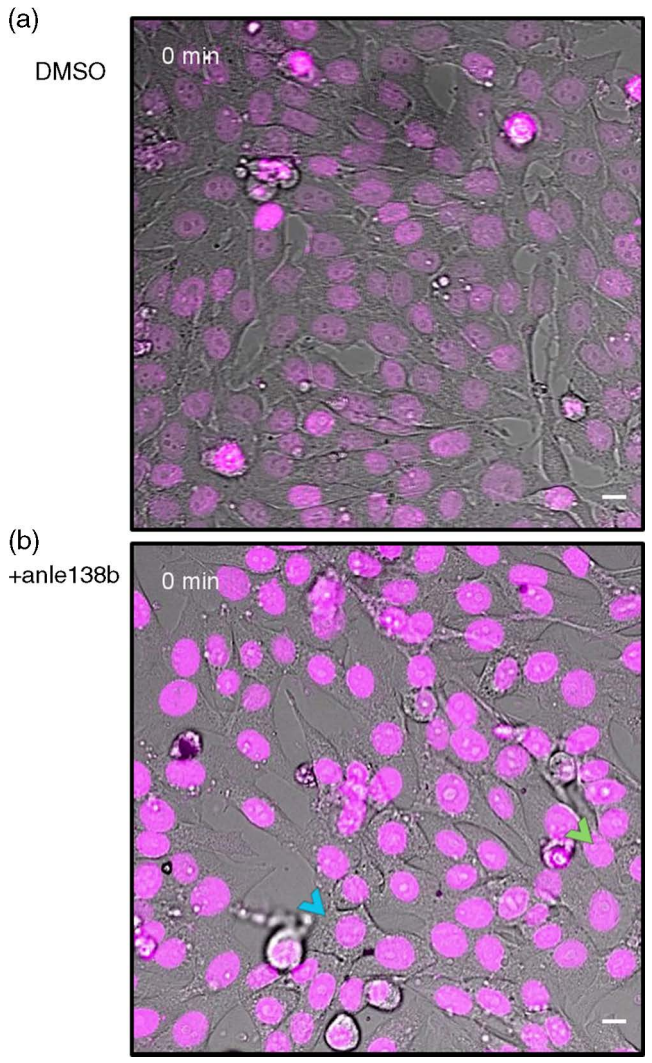

Time-lapse, live-cell imaging of anle138b-treated melanoma cells. (a) Live-cell imaging of WM983-B melanoma cells that had received DMSO only. (b) Live-cell imaging of WM983-B melanoma cells that were treated with 10 μM of anle138b for 48 h, with replenishment of 10 μM of the compound at 48 h and addition of the 5-580CP-Hoechst DNA probe. Images, captured every 10 min over the course of 15 h, are overlays of phase-contrast and 5-580CP-Hoechst dye-captured images (pseudocolored magenta). The triangle, colored turquoise, points to an area showing extensive vacuolization, and the green-colored triangle to a cell that failed to divide. Scale bar: 10 μm. DMSO, dimethyl sulfoxide.

measures of Parkinson's disease [26]. The upregulation of the QPCT enzyme is of interest not only because of its link to Alzheimer's and Huntington's disease [27], but because it might also be a possible target for immunotherapy of the phagocytosis CD47-signal-regulatory protein-alpha (SIRP-α) pathway [28,29]. SCD, which was downregulated following a 72 h treatment with anle138b (Fig. 3c), is an endoplasmic reticulum enzyme that catalyzes the biosynthesis of monounsaturated from saturated fatty acids and acts as a modulator of α-synuclein-induced pathology [30]. SCD is expressed at high levels in the advanced stages of melanoma [31] and the microphthalmia-associated transcription factor is an activator of SCD [32]. It also has been shown that downregulating SCD ameliorates the cytotoxicity of α-synuclein and therefore, it has been suggested that SCD might be a new target for the treatment of Parkinson's disease [33]. FDPS, a key enzyme in sterol metabolism, was also one of the downregulated proteins identified by (MS)-based proteomics. The results of immunoblot analyses of WM983-B melanoma cells, treated for 48 h and 72 h with anle138b, confirmed that SCD1 as well as FDPS was downregulated in the WM983-B melanoma cells (Fig. 3c).

Because following anle138b treatment, the proteins in clusters 4 and 5 were upregulated both in the WM983-A primary and in the WM983-B metastatic melanoma cells, we queried the STRING database (https://string-db.org/) for these proteins. As shown in Fig. 3d, identified interaction networks were enriched in proteins involved in 'Autophagy of mitochondrion', 'Amyloidosis', 'Extracellular matrix organization', and 'IL-18 signaling pathway'.

Systemic treatment of metastatic human melanoma xenografts with anle138b affects the tumor tissue architecture and the intratumoral expression pattern and localization of α-synuclein

To determine to what extent anle138b treatment affected the morphology of the tumor cells and the α-synuclein protein and its localization in the WM983-B metastatic human melanoma xenografts, we probed two adjacent tissue sections, prepared from a tumor xenograft from a nude mouse that had not been treated and two adjacent sections from a tumor xenograft that had been treated with anle138b, with an antibody cocktail to the three human melanoma cell markers MART-1, tyrosinase, and gp100 and with an antibody to human α-synuclein. Images of a tissue section, prepared from a WM983-B tumor xenograft that received food pellets not containing anle138b, showed expression of the melanoma cell markers throughout the tumor tissue (Fig. 4a) and clear and pointed expression and localization of the α-synuclein protein in the melanoma cells (Fig. 4c). In comparison, images of a tissue section prepared from a WM983-B melanoma xenograft, resected from a mouse that for 10 days had received food pellets containing anle138b, showed significantly less expression of the melanoma cell markers and not throughout the entire tumor section (Fig. 4b), and also less expression of α-synuclein (Fig. 4d).

Systemic treatment of metastatic human melanoma xenografts with anle138b leads to downregulation of adhesion molecules and proteins in the oxidative stress/degradation pathway

To gain insights into changes that occurred in the proteome and transcriptome of metastatic human melanoma cells upon anle138b treatment, we generated

Fig. 3

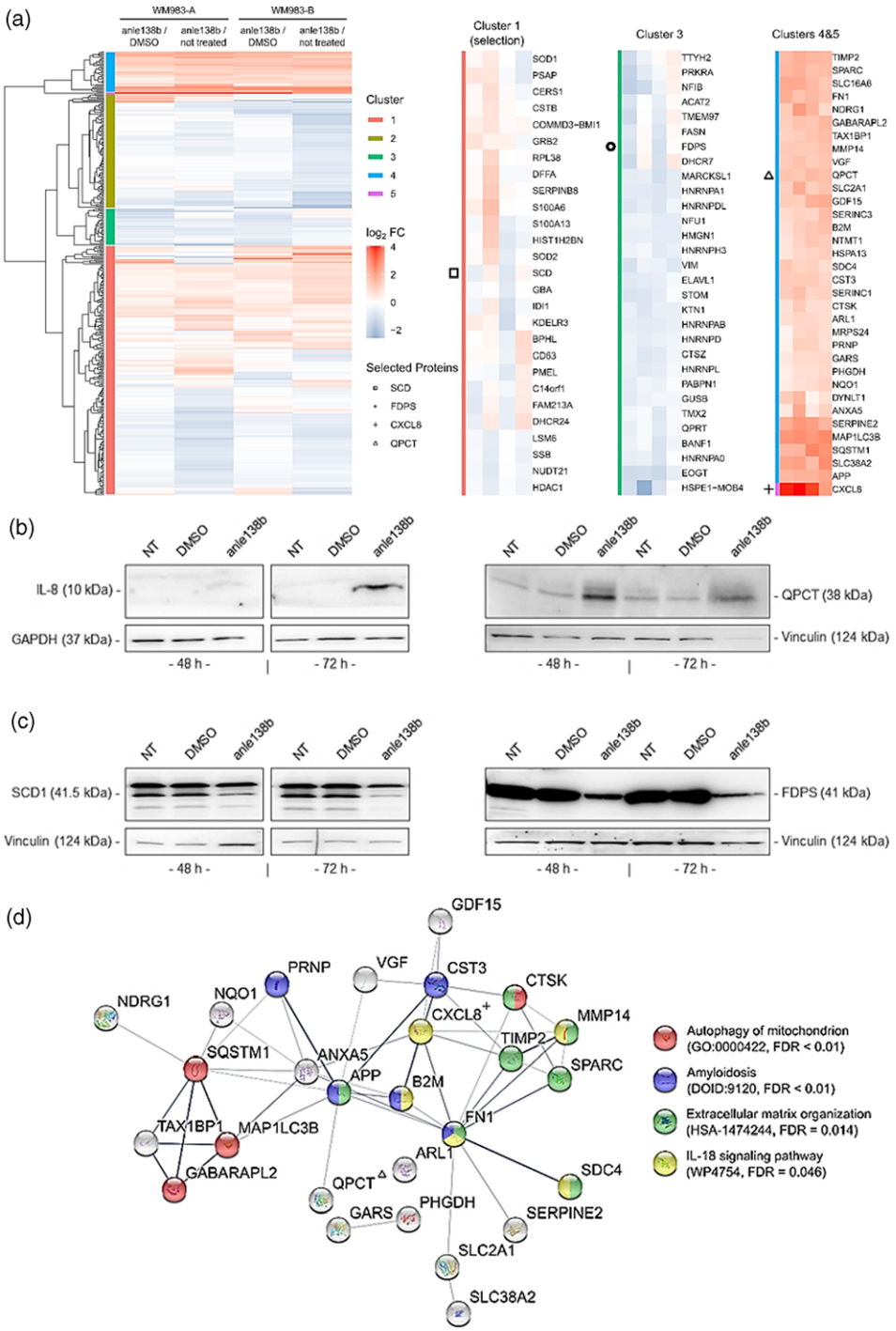

Proteome changes in primary and metastatic melanoma cell lines following treatment with anle138b. (a) Heatmap and hierarchical clustering of proteins, identified by MS-based proteomics analysis, that were dysregulated in the WM983-A primary and the WM983-B metastatic melanoma cells upon treatment with 10 μM of anle138b for 72 h, with replenishment of 10 μM of the compound at 48 h. Cluster 1 comprised 199 proteins. Thus, listed in the cluster 1 heatmap are only the proteins located above and below the protein SCD (SCD1). Listed in the entire cluster 3 heatmap are the proteins located above and below FDPS. Listed in combined clusters 4 and 5 are all proteins located above QPCT and IL-8 (CXCL8). (b) Immunoblot analysis of WM983-B melanoma cells that were treated with 10 μM of anle138b for 48 h or 72 h, with replenishment of 10 μM of the compound at 48 h. WM983-B melanoma cells that had received serum-free culture medium only (NT = nontreated) or serum-free culture medium containing DMSO served as controls. Immunoblots were probed with antibody to the proteins IL-8 (CXCL8) or QPCT, and with an anti-GAPDH or an anti-vinculin antibody for loading control. (c) Immunoblot analysis of WM983-B melanoma cells that were treated with 10 μM of anle138b for 48 h or 72 h, with replenishment of 10 μM of the compound at 48 h. WM983-B melanoma cells that had received serum-free culture medium only (NT = nontreated) or serum-free culture medium containing DMSO served as controls. Immunoblots were probed with antibody to the proteins SCD (SCD1) or FDPS, and with an anti-vinculin antibody for loading control. (d) Protein–protein interaction networks of the proteins in clusters 4 and 5 identified in the STRING database. DMSO, dimethyl sulfoxide; FDPS, farnesyl diphosphate synthase; MS, mass spectrometry; SCD, stearoyl-CoA desaturase.

Fig. 4

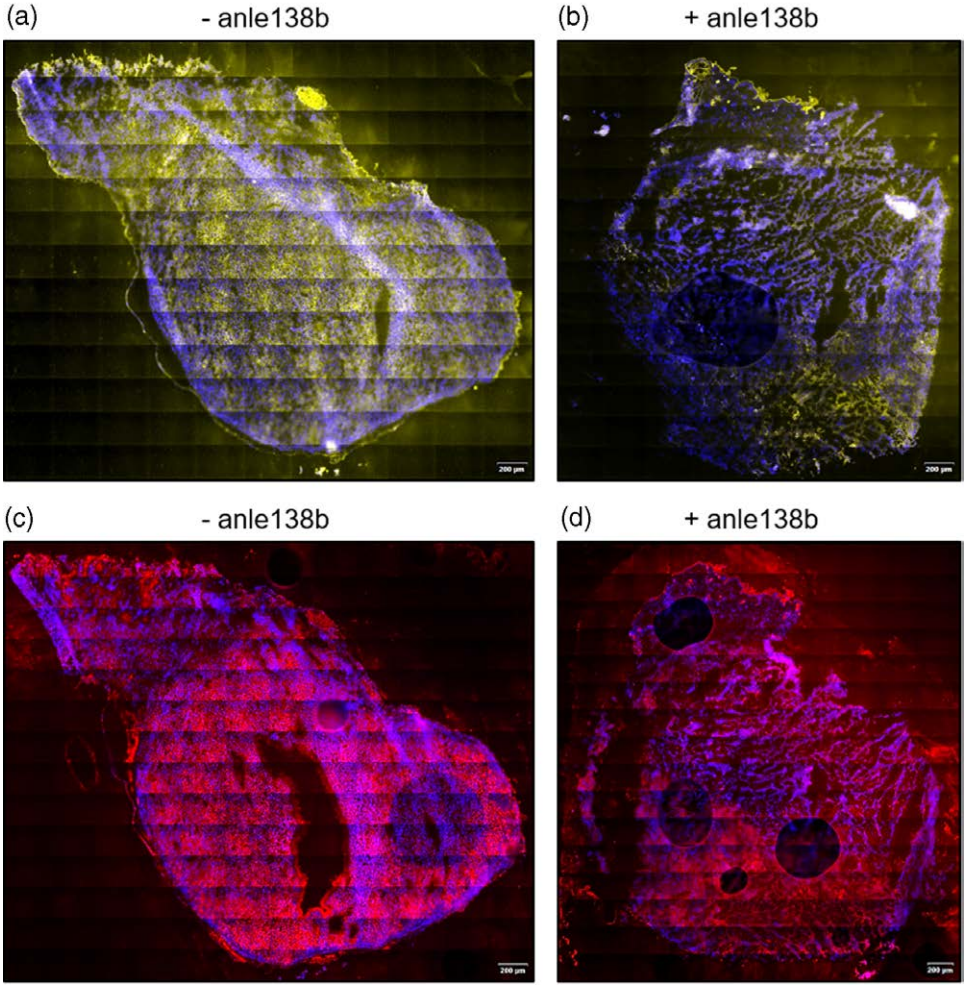

Morphology of human melanoma xenografts nontreated vs. treated with anle138b. (a) Expression of melanoma cell markers (MART-1, tyrosinase, gp100) in a tissue section, prepared from a WM983-B human melanoma xenograft resected from a nude mouse, which for 10 days had received food pellets not containing anle138b. (b) Expression of melanoma cell markers (MART-1, tyrosinase, gp100) in a tissue section, prepared from a WM983-B human melanoma xenograft resected from a nude mouse, which for 10 days had received food pellets containing anle138b. (c) Expression of α-synuclein in a tissue section, prepared from a WM983-B human melanoma xenograft resected from a nude mouse, which for 10 days had received food pellets not containing anle138b. (d) Expression of α-synuclein in a tissue section, prepared from a WM983-B human melanoma xenograft resected from a nude mouse, which for 10 days had received food pellets containing anle138b. The tumor xenograft tissue sections, probed with the human melanoma cell marker antibody cocktail (pseudocolored yellow) or with the anti-α-synuclein antibody (pseudocolored red), were counterstained with fluorescent DAPI (pseudocolored blue). (a–d) Scale bar: 200 μm.

subcutaneous WM983-B melanoma xenografts in nude mice and thereafter, treated the tumor-bearing animals systemically with anle138b for 14–16 days.

As depicted in scatter plots (Fig. 5a and b), fold changes of proteins, identified by both MS-based proteomics and RNA-seq analysis as being markedly changed (i.e. either upregulated or downregulated) in the human melanoma xenografts from the anle138b-treated versus from the nontreated nude mice, show a considerable degree of concordance. Identified as significantly downregulated in the anle138b-treated human melanoma tumor xenografts (Fig. 5b) were crystallin alpha B (CRYAB), cadherin 1 (CDH1), and the tumor protein D52-like 1 (TPD52L1), which is a member of the TPD52-like coiled-coil motif-bearing proteins that interact with 14-3-3 proteins [34]. Regarding CRYAB, a chaperone member of the small heat-shock protein family, it has been reported that it interacts with α-synuclein and that CRYAB and α-synuclein affect each other's properties [35]. With progression from early to advanced melanoma, a switch occurs from downregulation of E-cadherin (CDH1) to upregulation of N-cadherin expression [36,37], and loss of E-cadherin has been associated with ulcerated melanoma [38]. Immunohistochemistry analysis of WM983-B melanoma xenograft tissue sections confirmed that in

Fig. 5

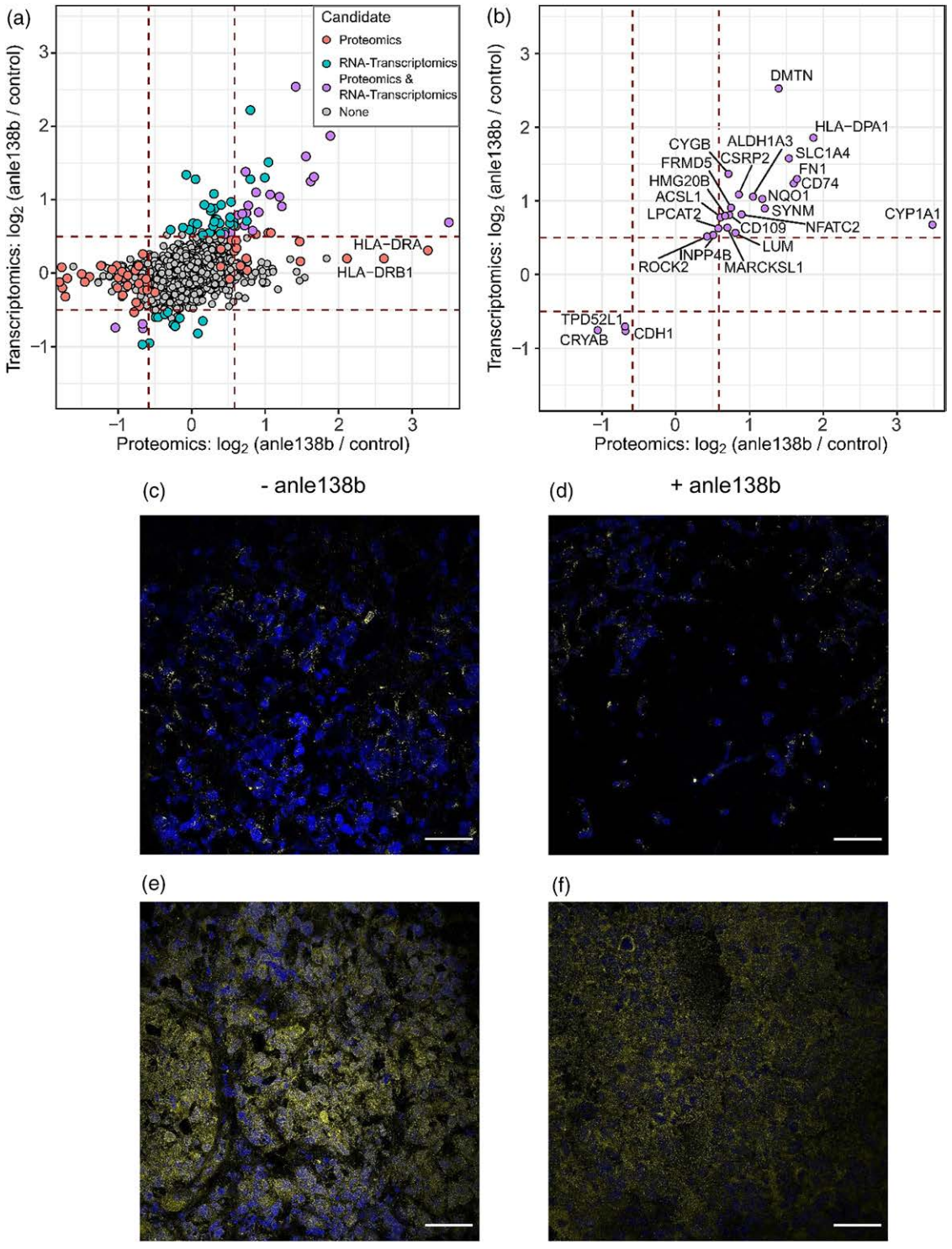

Proteome and transcriptome changes in human melanoma xenografts treated systemically with anle138b. (a) Comparison of log2FC changes of gene transcript/protein intensities identified by RNA-seq and MS-based proteomics. Candidate transcripts/proteins identified by RNA-seq, MS-based proteomics, or both are colored green, red, and purple, respectively. (b) Correlation of log2FC changes in gene transcript/protein intensity of gene transcripts/proteins selected based upon RNA-seq and MS-based proteomics analysis of WM983-B human melanoma xenografts resected from nude mice that had been treated systemically with anle138b, or had received food pellets not containing anle138b. (c) A tissue section from a nontreated WM983-B melanoma xenograft probed with an antibody to CRYAB. (d) A tissue section from an anle138b-treated WM983-B melanoma xenograft probed with a CRYAB antibody. (e) A tissue section from a nontreated WM983-B melanoma xenograft probed with an antibody to ALDH1A1. (f) A tissue section from an anle138b-treated WM983-B melanoma xenograft probed with an ALDH1A1 antibody. The anti-CRYAB and likewise, the anti-ALDH1A1 antibody-probed tumor xenograft tissue sections (pseudocolored yellow) were counterstained with fluorescent DAPI (pseudocolored blue). (c–f) Scale bar: 50 μm. MS, mass spectrometry.

comparison with a nontreated control tumor (Fig. 5c), expression of CRYAB was downregulated in an anle138b-treated tumor (Fig. 5d). Although not to the same extent as CRYAB, CDH1, and TPD52L1, downregulated in the anle138-treated WM983-B human melanoma tumor xenografts was also ALDH1A3, which is a member of the aldehyde dehydrogenase (ALDH) family of detoxifying enzymes that convert aldehydes to their carboxylic acids. It has been shown that ALDH1A1 and ALDH1A3 isozymes correlate with melanoma progression and that metastatic melanomas express the highest levels of ALDH [39,40], whereas in patients with Parkinson's disease, expression of ALDH1 is decreased in surviving dopamine neurons of the substantia nigra pars compacta [41]. As shown in Fig. 5f, immunohistochemistry analysis confirmed that a tissue section, prepared from an anle138b-treated WM983-B human melanoma xenograft, showed less expression of ALDHA1 in comparison with its high expression in a tissue section prepared from a melanoma xenograft that did not receive anle138b (Fig. 5e).

Systemic treatment of metastatic human melanoma xenografts with anle138b leads to a major upregulation of MHC class II molecules in the tumor cells

The results of the analysis of the transcriptomics data, the proteomics data or both revealed that significantly upregulated in the WM983-B metastatic human melanoma xenografts, resected from nude mice following their systemic treatment with anle138b, were as shown in Supplementary Fig. 1, Supplemental digital content 1, *http://links.lww.com/MR/A389*, molecules of the MHC class II HLA-DP and HLA-DR isotypes, class II transactivator (CIITA), the essential transactivator of MHC class II genes, and CD74, which plays an important role in the assembly and subcellular targeting of MHC class II complexes [42].

Verifying and confirming this finding, a tissue section prepared from one of the WM983-B human melanoma xenografts, resected from a nude mouse that had received food pellets mixed with anle138b, showed high-level MHC class II (HLA-DPB1) expression in the tumor cells Fig. 6b, whereas a tissue section prepared from a WM983-B human melanoma tumor xenograft of an animal that did not receive anle138b, showed little expression of this protein (Fig. 6a). Subsequently we performed a tissue microarray (TMA) analysis to determine whether in melanoma there might be a correlation or perhaps an inverse correlation between expression of α-synuclein and MHC class II antigen, MHC class I or MHC class II and MHC class I antigens. The results of probing a TMA, comprised of 39 cases of melanoma ranging from Stage II to Stage IV melanoma, with an antibody to human α-synuclein, to human MHC class II [HLA-DQ/DR/DP] or MHC class I [HLA-ABC] antigens, revealed that in some areas, encircled by a white line, in tissue sections from several of the melanoma TMA cores in which α-synuclein was strongly expressed, there was less expression of MHC II protein, or vice versa (Fig. 6c). Images of all of the TMA cores probed with antibody to human α-synuclein, MHC class II or MHC class I antigen are shown in Supplementary Fig. S2A–D, Supplemental digital content 2, *http://links.lww.com/MR/A390*.

In addition to the MHC class II molecules, FN1 was another protein, whose expression was upregulated in the anle138b-treated metastatic human melanoma xenografts. FN1, a high-molecular weight extracellular matrix protein, is involved in many processes including cell adhesion, cell motility, and maintenance of cell shape. It is possible, that following interference of oligomeric α-synuclein with the DPP compound anle138b, the subsequent dysregulation of autophagy in the melanoma cells, and as part of or a consequence of it, the cells losing their cell-matrix adhesion led compared with the control (Supplementary Fig. 3A, Supplemental digital content 3, *http://links.lww.com/MR/A391*), to an increase in FN1 expression in the melanoma xenografts (Supplementary Fig. 3B, Supplemental digital content 3, *http://links.lww.com/MR/A391*), and also as shown in Supplementary Fig. 3C, Supplemental digital content 3, *http://links.lww.com/MR/A391*, in WM983-B human melanoma cells treated in vitro with anle138b for 48 h and 72 h. A query of the STRING database for the proteins upregulated in the anle138b-treated WM983-B metastatic human melanoma xenografts, identified interaction networks that were enriched in proteins of the 'MHC class II protein complex' and the 'Extracellular space' (Supplementary Fig. 3D, Supplemental digital content 3, *http://links.lww.com/MR/A391*).

Regarding three of the proteins namely, CRYAB, ALDH1A1, and MHC II, we identified by MS-based proteomics and/or RNA-seq analysis in the WM983-B tumor-bearing xenografts, we also determined by CTCF (Supplementary Fig. 4A–C, Supplemental digital content 4, *http://links.lww.com/MR/A392*), their level of expression in tissue sections prepared from WM983-B tumor xenografts that were resected from several of the mice that received food pellets not containing or containing anle138b.

Discussion

Over the past decade, treatment options for patients with advanced melanoma have expanded [43], and for the years 2013 through 2017, the overall melanoma mortality rate dropped annually by 7% [44]; nonetheless, the long-term survival rate for patients with advanced melanoma is still low.

It has been reported that, with relevance to Parkinson's disease, an inter-relationship exists between α-synuclein and the autophagy-lysosomal pathway [45]; and that peptides derived from two regions of α-synuclein produce

Fig. 6

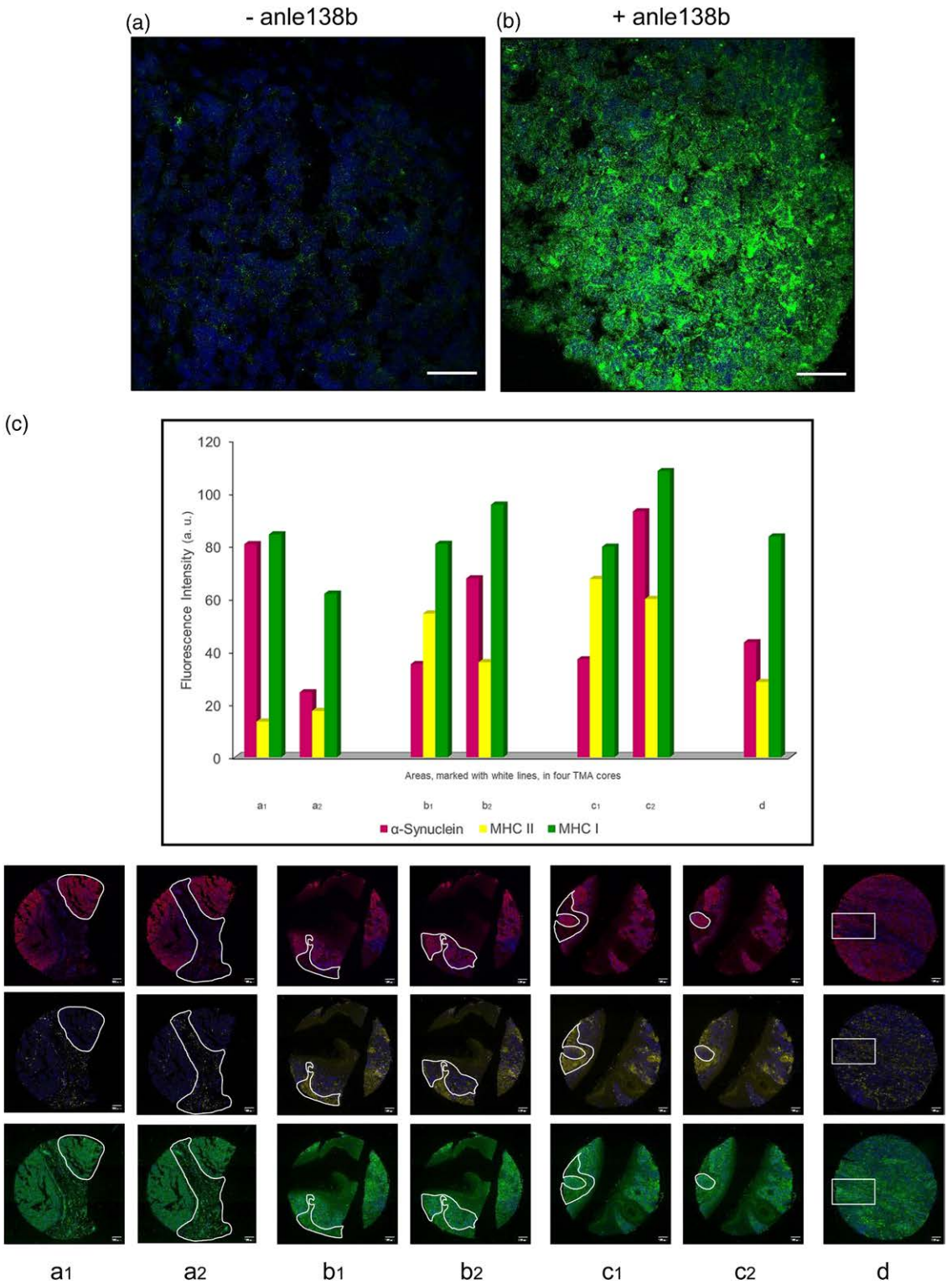

Upregulation of MHC class II antigen in human melanoma xenografts treated systemically with anle138b, and expression of α-synuclein, MHC class II, and MHC class I proteins in melanoma TMA cores. (a) A tissue section from a nontreated WM983-B tumor xenograft probed with an antibody to human MHC class II (HLA-DPB1) protein (pseudocolored green). (b) A tissue section from an anle138b-treated WM983-B tumor xenograft probed with an antibody to human MHC class II (HLA-DPB1) protein (pseudocolored green). (c) Fluorescence intensity level of expression of proteins – α-synuclein (pseudocolored red), MHC II (pseudocolored yellow), MHC I (pseudocolored green) – in areas, encircled by a white line, in tissue sections from three of the Stage II and from one of the Stage IV melanoma TMA cores in which α-synuclein or vice versa, MHC II, or MHC I protein was expressed more strongly. TMA, tissue microarray.

immune responses in patients with Parkinson's disease and that these immune responses have both MHC class I and MHC class II-restricted components [46]. Previously, we reported that high-level expression of α-synuclein is essential for the survival of primary and metastatic human melanoma because it serves as a pertinent guardian, which ensures that autophagy in these malignant cells is neither too high nor too low [8].

Our finding that anle138b treatment of the high-level α-synuclein-expressing WM983-B melanoma cells led to a substantial release of α-synuclein into the cell culture supernatant, whereas treatment with the autophagy inducer, rapamycin, did not (Fig. 1b), may be due to the fact that anle138b interferes with and reduces oligomeric and fibrillary α-synuclein aggregates to low-molecular weight forms, that unlike aggregated α-synuclein [47,48], are not cleared mainly by autophagy. Experimental studies, performed in cell culture, in tumor xenograft models or in both, has provided ample evidence for a connection between autophagy and cell migration/adhesion [49] and the extracellular matrix [50,51]. Thus, it is not entirely surprising that upon treatment of the primary and metastatic human melanoma cells and the metastatic melanoma xenografts with anle138b, α-synuclein could no longer safeguard melanoma cell autophagy; and perhaps as one of the first consequences, impaired autophagic flux led to degradation of the extracellular matrix and as part of this, the extracellular matrix/scaffold protein FN1 became upregulated. Of interest too is that in the WM983-A and WM983-B melanoma cell lines and in the WM983-B human melanoma tumor xenografts treated with anle138b, proteins important in metabolic processes were impaired. Another intriguing aspect regarding expression of α-synuclein, MHC class II, and MHC class I antigens are the results of our immunohistochemical analysis of the melanoma TMA, which show that in some of the tissue cores and an area therein, in which α-synuclein is expressed strongly, MHC class II (HLA DQ/DR/DP) protein is not strongly expressed or vice versa (Fig. 6c; Supplementary Fig. 2A–D, Supplemental digital content 2, *http://links.lww.com/MR/A390*).

It has been reported that microglial MHC class II plays a role in the activation of innate and adaptive immune responses to α-synuclein [52] and that peptides, derived from two regions of α-synuclein produce immune responses in patients with Parkinson's disease, are recognized by T cells [46]; however, regarding advanced melanoma, a link between α-synuclein and MHC class II antigens has not been described before. Given our finding, that as a result of systemic treatment with anle138b, MHC class II but not MHC class I proteins were upregulated to a significant extent in the high-level α-synuclein-expressing human melanoma xenografts might be linked to the fact that lysosomal degradation products, recognized by CD4+ T cells, are presented on MHC class II molecules [53] whereas proteasomal degradation products, recognized by CD8+ T cells, are presented on MHC class I molecules.

Conclusion

Immune evasion is one of the hallmarks of melanoma in its advances stages. Our finding that interfering with oligomerized α-synuclein in primary and even more so in metastatic melanoma cells leads to a major upregulation of MHC class II antigens, suggests that prior to immunotherapy, and in particular prior to therapies with immune checkpoint inhibitors, treatment with a small-molecule compound that substantially reduces oligomeric to monomeric α-synuclein, may increase the response rate to these treatments.

Acknowledgements

This work was supported by a grant (2018.047.1) from the Wilhelm Sander-Stiftung (to D.B.), funds from the Max Planck Society (to C.G., D.B. and H.U.) and the German Research Foundation (DFG) Cluster of Excellence 2067/1-390729940 (to C.G.) and SFB1286 (to H.U.). We thank P. Lenart and A. Politi for assistance with the live-cell imaging of the human melanoma cells and creation of the videos; T. Boothe for assistance with capturing the virtual slide images of the human melanoma tissue sections; S. Luthin for having performed the transcriptome study (RNA-seq); S. König, M. Raabe, and U. Pleßmann for technical support with the LC-MS/MS analysis; E. Gerhardt for assistance with the ELISA assay.

C.F., I.S., K.-T.P., S.R., N.W., and D.B. performed experiments. O.S. and I.S. performed bioinformatics analyses. C.G. and A.L. provided the anle138b compound. H.U. supervised the MS-based proteomics analysis. D.B. and C.G. conceived of the study. D.B. designed and supervised the study, and wrote the manuscript. All authors read and edited the manuscript.

The LC-MS/MS proteomics datasets have been deposited in the ProteomeXchange Consortium via the PRIDE partner repository with the dataset identifier PXD030615. The RNA-seq datasets, deposited in the NCBI Gene Expression Omnibus (GEO), are accessible through GEO Series accession number GSE240854.

Conflicts of interest

C.G. is cofounder and shareholder of MODAG GmbH. S.R. and A.L. are part-time employees of MODAG GmbH and beneficiaries of the phantom share program of MODAG GmbH. D.B., C.G., S.R., and A.L. are inventors on a patent application (PCT/EP2018/062236) related to the use of the anle138b compound in the treatment or prevention of melanoma. There are no conflicts of interest for the remaining authors.

References

1 Larkin J, Chiarion-Sileni V, Gonzalez R, Grob JJ, Rutkowski P, Lao CD, *et al*. Five-year survival with combined nivolumab and ipilimumab in advanced melanoma. *N Engl J Med* 2019; **381**:1535–1546.

2 Gellrich FF, Schmitz M, Beissert S, Meier F. Anti-PD-1 and novel combinations in the treatment of melanoma–an update. *J Clin Med* 2020; **9**:223.

3 Lazova R, Klump V, Pawelek J. Autophagy in cutaneous malignant melanoma. *J Cutan Pathol* 2010; **37**:256–268.

4 Ma XH, Piao S, Wang D, McAfee QW, Nathanson KL, Lum JJ, *et al*. Measurements of tumor cell autophagy predict invasiveness, resistance to chemotherapy, and survival in melanoma. *Clin Cancer Res* 2011; **17**:3478–3489.

5 Ma XH, Piao SF, Dey S, McAfee Q, Karakousis G, Villanueva J, *et al*. Targeting ER stress-induced autophagy overcomes BRAF inhibitor resistance in melanoma. *J Clin Invest* 2014; **124**:1406–1417.

6 Xie X, Koh JY, Price S, White E, Mehnert JM. Atg7 overcomes senescence and promotes growth of BrafV600E-driven melanoma. *Cancer Discov* 2015; **5**:410–423.

7 Surguchov A, Surguchev AA. Association between Parkinson's disease and cancer: new findings and possible mediators. *Int J Mol Sci* 2024; **25**:3899.

8 Turriani E, Lazaro DF, Ryazanov S, Leonov A, Giese A, Schon M, *et al*. Treatment with diphenyl-pyrazole compound anle138b/c reveals that alpha-synuclein protects melanoma cells from autophagic cell death. *Proc Natl Acad Sci U S A* 2017; **114**:E4971–E4977.

9 Wagner J, Ryazanov S, Leonov A, Levin J, Shi S, Schmidt F, *et al*. Anle138b: a novel oligomer modulator for disease-modifying therapy of neurodegenerative diseases such as prion and Parkinson's disease. *Acta Neuropathol* 2013; **125**:795–813.

10 Lee J, Sung KW, Bae EJ, Yoon D, Kim D, Lee JS, *et al*. Targeted degradation of α-synuclein aggregates in Parkinson's disease using the AUTOTAC technology. *Mol Neurodegener* 2023; **18**:41.

11 Silbern I, Fang P, Ji Y, Christof L, Urlaub H, Pan KT. Relative quantification of phosphorylated and glycosylated peptides from the same sample using isobaric chemical labelling with a two-step enrichment strategy. *Methods Mol Biol* 2021; **2228**:185–203.

12 McAlister GC, Nusinow DP, Jedrychowski MP, Wuhr M, Huttlin EL, Erickson BK, *et al*. MultiNotch MS3 enables accurate, sensitive, and multiplexed detection of differential expression across cancer cell line proteomes. *Anal Chem* 2014; **86**:7150–7158.

13 Dobin A, Davis CA, Schlesinger F, Drenkow J, Zaleski C, Jha S, *et al*. STAR: ultrafast universal RNA-seq aligner. *Bioinformatics* 2013; **29**:15–21.

14 Liao Y, Smyth GK, Shi W. featureCounts: an efficient general purpose program for assigning sequence reads to genomic features. *Bioinformatics* 2014; **30**:923–930.

15 Love MI, Huber W, Anders S. Moderated estimation of fold change and dispersion for RNA-seq data with DESeq2. *Genome Biol* 2014; **15**:550.

16 Durinck S, Spellman PT, Birney E, Huber W. Mapping identifiers for the integration of genomic datasets with the R/Bioconductor package biomaRt. *Nat Protoc* 2009; **4**:1184–1191.

17 Bankhead P, Loughrey MB, Fernandez JA, Dombrowski Y, McArt DG, Dunne PD, *et al*. QuPath: open source software for digital pathology image analysis. *Sci Rep* 2017; **7**:16878.

18 Danzer KM, Kranich LR, Ruf WP, Cagsal-Getkin O, Winslow AR, Zhu L, *et al*. Exosomal cell-to-cell transmission of alpha synuclein oligomers. *Mol Neurodegener* 2012; **7**:42.

19 Hardwick JS, Kuruvilla FG, Tong JK, Shamji AF, Schreiber SL. Rapamycin-modulated transcription defines the subset of nutrient-sensitive signaling pathways directly controlled by the Tor proteins. *Proc Natl Acad Sci U S A* 1999; **96**:14866–14870.

20 Cox D, Selig E, Griffin MD, Carver JA, Ecroyd H. Small heat-shock proteins prevent alpha-synuclein aggregation via transient interactions and their efficacy is affected by the rate of aggregation. *J Biol Chem* 2016; **291**:22618–22629.

21 Pineda CT, Potts PR. Oncogenic MAGEA-TRIM28 ubiquitin ligase downregulates autophagy by ubiquitinating and degrading AMPK in cancer. *Autophagy* 2015; **11**:844–846.

22 Czerwinska P, Jaworska AM, Wlodarczyk NA, Mackiewicz AA. Melanoma stem cell-like phenotype and significant suppression of immune response within a tumor are regulated by TRIM28 protein. *Cancers (Basel)* 2020; **12**:2998.

23 Bucevicius J, Keller-Findeisen J, Gilat T, Hell SW, Lukinavicius G. Rhodamine-Hoechst positional isomers for highly efficient staining of heterochromatin. *Chem Sci* 2019; **10**:1962–1970.

24 Singh RK, Varney ML, Bucana CD, Johansson SL. Expression of interleukin-8 in primary and metastatic malignant melanoma of the skin. *Melanoma Res* 1999; **9**:383–387.

25 Nurnberg W, Tobias D, Otto F, Henz BM, Schadendorf D. Expression of interleukin-8 detected by in situ hybridization correlates with worse prognosis in primary cutaneous melanoma. *J Pathol* 1999; **189**:546–551.

26 Eidson LN, Kannarkat GT, Barnum CJ, Chang J, Chung J, Caspell-Garcia C, *et al*. Candidate inflammatory biomarkers display unique relationships with alpha-synuclein and correlate with measures of disease severity in subjects with Parkinson's disease. *J Neuroinflammation* 2017; **14**:164.

27 Jimenez-Sanchez M, Lam W, Hannus M, Sonnichsen B, Imarisio S, Fleming A, *et al*. siRNA screen identifies QPCT as a druggable target for Huntington's disease. *Nat Chem Biol* 2015; **11**:347–354.

28 Logtenberg MEW, Scheeren FA, Schumacher TN. The CD47-SIRPalpha immune checkpoint. *Immunity* 2020; **52**:742–752.

29 Feng R, Zhao H, Xu J, Shen C. CD47: the next checkpoint target for cancer immunotherapy. *Crit Rev Oncol Hematol* 2020; **152**:103014.

30 Nicholatos JW, Groot J, Dhokai S, Tran D, Hrdlicka L, Carlile TM, *et al*. SCD inhibition protects from alpha-synuclein-induced neurotoxicity but is toxic to early neuron cultures. *eNeuro* 2021; **8**:ENEURO.0166-21.2021.

31 Pisanu ME, Maugeri-Sacca M, Fattore L, Bruschini S, De Vitis C, Tabbi E, *et al*. Inhibition of stearoyl-CoA desaturase 1 reverts BRAF and MEK inhibition-induced selection of cancer stem cells in BRAF-mutated melanoma. *J Exp Clin Cancer Res* 2018; **37**:318.

32 Vivas-Garcia Y, Falletta P, Liebing J, Louphrasitthiphol P, Feng Y, Chauhan J, *et al*. Lineage-restricted regulation of SCD and fatty acid saturation by MITF controls melanoma phenotypic plasticity. *Mol Cell* 2020; **77**:120–137.e9.

33 Fanning S, Haque A, Imberdis T, Baru V, Barrasa MI, Nuber S, *et al*. Lipidomic analysis of alpha-synuclein neurotoxicity identifies stearoyl CoA desaturase as a target for Parkinson treatment. *Mol Cell* 2019; **73**:1001–1014.e8.

34 Boutros R, Bailey AM, Wilson SH, Byrne JA. Alternative splicing as a mechanism for regulating 14-3-3 binding: interactions between hD53 (TPD52L1) and 14-3-3 proteins. *J Mol Biol* 2003; **332**:675–687.

35 Rekas A, Adda CG, Andrew Aquilina J, Barnham KJ, Sunde M, Galatis D, *et al*. Interaction of the molecular chaperone alphaB-crystallin with alpha-synuclein: effects on amyloid fibril formation and chaperone activity. *J Mol Biol* 2004; **340**:1167–1183.

36 Danen EH, de Vries TJ, Morandini R, Ghanem GG, Ruiter DJ, van Muijen GN. E-cadherin expression in human melanoma. *Melanoma Res* 1996; **6**:127–131.

37 Kuphal S, Bosserhoff AK. E-cadherin cell-cell communication in melanogenesis and during development of malignant melanoma. *Arch Biochem Biophys* 2012; **524**:43–47.

38 Bonnelykke-Behrndtz ML, Steiniche T, Norgaard P, Danielsen AV, Damsgaard TE, Christensen IJ, *et al*. Loss of E-cadherin as part of a migratory phenotype in melanoma is associated with ulceration. *Am J Dermatopathol* 2017; **39**:672–678.

39 Samson JM, Ravindran Menon D, Smith DE, Baird E, Kitano T, Gao D, *et al*. Clinical implications of ALDH1A1 and ALDH1A3 mRNA expression in melanoma subtypes. *Chem Biol Interact* 2019; **314**:108822.

40 Dinavahi SS, Gowda R, Gowda K, Bazewicz CG, Chirasani VR, Battu MB, *et al*. Development of a novel multi-isoform ALDH inhibitor effective as an antimelanoma agent. *Mol Cancer Ther* 2020; **19**:447–459.

41 Galter D, Buervenich S, Carmine A, Anvret M, Olson L. ALDH1 mRNA: presence in human dopamine neurons and decreases in substantia nigra in Parkinson's disease and in the ventral tegmental area in schizophrenia. *Neurobiol Dis* 2003; **14**:637–647.

42 Axelrod ML, Cook RS, Johnson DB, Balko JM. Biological consequences of MHC-II expression by tumor cells in cancer. *Clin Cancer Res* 2019; **25**:2392–2402.

43 Robert C. A decade of immune-checkpoint inhibitors in cancer therapy. *Nat Commun* 2020; **11**:3801.

44 Siegel RL, Miller KD, Jemal A. Cancer statistics, 2020. *CA Cancer J Clin* 2020; **70**:7–30.

45 Xilouri M, Brekk OR, Stefanis L. Autophagy and alpha-synuclein: relevance to Parkinson's disease and related synucleopathies. *Mov Disord* 2016; **31**:178–192.

46 Sulzer D, Alcalay RN, Garretti F, Cote L, Kanter E, Agin-Liebes J, *et al*. T cells from patients with Parkinson's disease recognize alpha-synuclein peptides. *Nature* 2017; **546**:656–661.

47 Webb JL, Ravikumar B, Atkins J, Skepper JN, Rubinsztein DC. Alpha-synuclein is degraded by both autophagy and the proteasome. *J Biol Chem* 2003; **278**:25009–25013.

48 Pantazopoulou M, Brembati V, Kanellidi A, Bousset L, Melki R, Stefanis L. Distinct alpha-synuclein species induced by seeding are selectively cleared by the lysosome or the proteasome in neuronally differentiated SH-SY5Y cells. *J Neurochem* 2021; **156**:880–896.

49 Kenific CM, Wittmann T, Debnath J. Autophagy in adhesion and migration. *J Cell Sci* 2016; **129**:3685–3693.
50 Fung C, Lock R, Gao S, Salas E, Debnath J. Induction of autophagy during extracellular matrix detachment promotes cell survival. *Mol Biol Cell* 2008; **19**:797–806.
51 Schaefer L, Dikic IA. Instructions from the extracellular matrix. *Matrix Biol* 2021; **100–101**:1–8.
52 Harms AS, Cao S, Rowse AL, Thome AD, Li X, Mangieri LR, *et al*. MHCII is required for alpha-synuclein-induced activation of microglia, CD4 T cell proliferation, and dopaminergic neurodegeneration. *J Neurosci* 2013; **33**:9592–9600.
53 Roche PA, Furuta K. The ins and outs of MHC class II-mediated antigen processing and presentation. *Nat Rev Immunol* 2015; **15**:203–216.